

Measurements of Absolute Branching Fractions of Fourteen Exclusive Hadronic D Decays to η

M. Ablikim¹, M. N. Achasov^{10,c}, P. Adlarson⁶⁴, S. Ahmed¹⁵, M. Albrecht⁴, A. Amoroso^{63A,63C}, Q. An^{60,48}, Anita²¹, X. H. Bai⁵⁴, Y. Bai⁴⁷, O. Bakina²⁹, R. Baldini Ferroli^{23A}, I. Balossino^{24A}, Y. Ban^{38,k}, K. Begzsuren²⁶, J. V. Bennett⁵, N. Berger²⁸, M. Bertani^{23A}, D. Bettoni^{24A}, F. Bianchi^{63A,63C}, J. Biernat⁶⁴, J. Bloms⁵⁷, A. Bortone^{63A,63C}, I. Boyko²⁹, R. A. Briere⁵, H. Cai⁶⁵, X. Cai^{1,48}, A. Calcaterra^{23A}, G. F. Cao^{1,52}, N. Cao^{1,52}, S. A. Cetin^{51B}, J. F. Chang^{1,48}, W. L. Chang^{1,52}, G. Chelkov^{29,b}, D. Y. Chen⁶, G. Chen¹, H. S. Chen^{1,52}, M. L. Chen^{1,48}, S. J. Chen³⁶, X. R. Chen²⁵, Y. B. Chen^{1,48}, W. S. Cheng^{63C}, G. Cibinetto^{24A}, F. Cossio^{63C}, X. F. Cui³⁷, H. L. Dai^{1,48}, J. P. Dai^{42,g}, X. C. Dai^{1,52}, A. Dbeysi¹⁵, R. B. de Boer⁴, D. Dedovich²⁹, Z. Y. Deng¹, A. Denig²⁸, I. Denysenko²⁹, M. Destefanis^{63A,63C}, F. De Mori^{63A,63C}, Y. Ding³⁴, C. Dong³⁷, J. Dong^{1,48}, L. Y. Dong^{1,52}, M. Y. Dong^{1,48,52}, S. X. Du⁶⁸, J. Fang^{1,48}, S. S. Fang^{1,52}, Y. Fang¹, R. Farinelli^{24A}, L. Fava^{63B,63C}, F. Feldbauer⁴, G. Felici^{23A}, C. Q. Feng^{60,48}, M. Fritsch⁴, C. D. Fu¹, Y. Fu¹, X. L. Gao^{60,48}, Y. Gao^{38,k}, Y. Gao⁶¹, Y. G. Gao⁶, I. Garzia^{24A,24B}, E. M. Gersabeck⁵⁵, A. Gilman⁵⁶, K. Goetzen¹¹, L. Gong³⁷, W. X. Gong^{1,48}, W. Gradl²⁸, M. Greco^{63A,63C}, L. M. Gu³⁶, M. H. Gu^{1,48}, S. Gu², Y. T. Gu¹³, C. Y. Guan^{1,52}, A. Q. Guo²², L. B. Guo³⁵, R. P. Guo⁴⁰, Y. P. Guo^{9,h}, Y. P. Guo²⁸, A. Guskov²⁹, S. Han⁶⁵, T. T. Han⁴¹, T. Z. Han^{9,h}, X. Q. Hao¹⁶, F. A. Harris⁵³, K. L. He^{1,52}, F. H. Heinsius⁴, T. Held⁴, Y. K. Heng^{1,48,52}, M. Himmelreich^{11,f}, T. Holtmann⁴, Y. R. Hou⁵², Z. L. Hou¹, H. M. Hu^{1,52}, J. F. Hu^{42,g}, T. Hu^{1,48,52}, Y. Hu¹, G. S. Huang^{60,48}, L. Q. Huang⁶¹, X. T. Huang⁴¹, Y. P. Huang¹, Z. Huang^{38,k}, N. Huesken⁵⁷, T. Hussain⁶², W. Ikegami Andersson⁶⁴, W. Imoehl²², M. Irshad^{60,48}, S. Jaeger⁴, S. Janchiv^{26,j}, Q. Ji¹, Q. P. Ji¹⁶, X. B. Ji^{1,52}, X. L. Ji^{1,48}, H. B. Jiang⁴¹, X. S. Jiang^{1,48,52}, X. Y. Jiang³⁷, J. B. Jiao⁴¹, Z. Jiao¹⁸, S. Jin³⁶, Y. Jin⁵⁴, T. Johansson⁶⁴, N. Kalantar-Nayestanaki³¹, X. S. Kang³⁴, R. Kappert³¹, M. Kavatsyuk³¹, B. C. Ke^{43,1}, I. K. Keshk⁴, A. Khoukaz⁵⁷, P. Kiese²⁸, R. Kiuchi¹, R. Kliemt¹¹, L. Koch³⁰, O. B. Kolcu^{51B,e}, B. Kopf⁴, M. Kuemmel⁴, M. Kuessner⁴, A. Kupsc⁶⁴, M. G. Kurth^{1,52}, W. Kühn³⁰, J. J. Lane⁵⁵, J. S. Lange³⁰, P. Larin¹⁵, L. Lavezzi^{63C}, H. Leithoff²⁸, M. Lellmann²⁸, T. Lenz²⁸, C. Li³⁹, C. H. Li³³, Cheng Li^{60,48}, D. M. Li⁶⁸, F. Li^{1,48}, G. Li¹, H. B. Li^{1,52}, H. J. Li^{9,h}, J. L. Li⁴¹, J. Q. Li⁴, Ke Li¹, L. K. Li¹, Lei Li³, P. L. Li^{60,48}, P. R. Li³², S. Y. Li⁵⁰, W. D. Li^{1,52}, W. G. Li¹, X. H. Li^{60,48}, X. L. Li⁴¹, Z. B. Li⁴⁹, Z. Y. Li⁴⁹, H. Liang^{60,48}, H. Liang^{1,52}, Y. F. Liang⁴⁵, Y. T. Liang²⁵, L. Z. Liao^{1,52}, J. Libby²¹, C. X. Lin⁴⁹, B. Liu^{42,g}, B. J. Liu¹, C. X. Liu¹, D. Liu^{60,48}, D. Y. Liu^{42,g}, F. H. Liu⁴⁴, Fang Liu¹, Feng Liu⁶, H. B. Liu¹³, H. M. Liu^{1,52}, Huanhuan Liu¹, Huihui Liu¹⁷, J. B. Liu^{60,48}, J. Y. Liu^{1,52}, K. Liu¹, K. Y. Liu³⁴, Ke Liu⁶, L. Liu^{60,48}, Q. Liu⁵², S. B. Liu^{60,48}, Shuai Liu⁴⁶, T. Liu^{1,52}, X. Liu³², Y. B. Liu³⁷, Z. A. Liu^{1,48,52}, Z. Q. Liu⁴¹, Y. F. Long^{38,k}, X. C. Lou^{1,48,52}, F. X. Lu¹⁶, H. J. Lu¹⁸, J. D. Lu^{1,52}, J. G. Lu^{1,48}, X. L. Lu¹, Y. Lu¹, Y. P. Lu^{1,48}, C. L. Luo³⁵, M. X. Luo⁶⁷, P. W. Luo⁴⁹, T. Luo^{9,h}, X. L. Luo^{1,48}, S. Lusso^{63C}, X. R. Lyu⁵², F. C. Ma³⁴, H. L. Ma¹, L. L. Ma⁴¹, M. M. Ma^{1,52}, Q. M. Ma¹, R. Q. Ma^{1,52}, R. T. Ma⁵², X. N. Ma³⁷, X. X. Ma^{1,52}, X. Y. Ma^{1,48}, Y. M. Ma⁴¹, F. E. Maas¹⁵, M. Maggiora^{63A,63C}, S. Maldaner²⁸, S. Malde⁵⁸, Q. A. Malik⁶², A. Mangoni^{23B}, Y. J. Mao^{38,k}, Z. P. Mao¹, S. Marcello^{63A,63C}, Z. X. Meng⁵⁴, J. G. Messchendorp³¹, G. Mezzadri^{24A}, T. J. Min³⁶, R. E. Mitchell²², X. H. Mo^{1,48,52}, Y. J. Mo⁶, N. Yu. Muchnoi^{10,c}, H. Muramatsu⁵⁶, S. Nakhoul^{11,f}, Y. Nefedov²⁹, F. Nerling^{11,f}, I. B. Nikolaev^{10,c}, Z. Ning^{1,48}, S. Nisar^{8,i}, S. L. Olsen⁵², Q. Ouyang^{1,48,52}, S. Pacetti^{23B,23C}, X. Pan^{9,h}, Y. Pan⁵⁵, A. Pathak¹, P. Patteri^{23A}, M. Pelizaeus⁴, H. P. Peng^{60,48}, K. Peters^{11,f}, J. Pettersson⁶⁴, J. L. Ping³⁵, R. G. Ping^{1,52}, A. Pitka⁴, R. Poling⁵⁶, V. Prasad^{60,48}, H. Qi^{60,48}, H. R. Qi⁵⁰, M. Qi³⁶, T. Y. Qi⁹, T. Y. Qi², S. Qian^{1,48}, W.-B. Qian⁵², Z. Qian⁴⁹, C. F. Qiao⁵², L. Q. Qin¹², X. P. Qin¹³, X. S. Qin⁴, Z. H. Qin^{1,48}, J. F. Qiu¹, S. Q. Qu³⁷, K. H. Rashid⁶², K. Ravindran²¹, C. F. Redmer²⁸, A. Rivetti^{63C}, V. Rodin³¹, M. Rolo^{63C}, G. Rong^{1,52}, Ch. Rosner¹⁵, M. Rump⁵⁷, A. Sarantsev^{29,d}, Y. Schelhaas²⁸, C. Schnier⁴, K. Schoenning⁶⁴, D. C. Shan⁴⁶, W. Shan¹⁹, X. Y. Shan^{60,48}, M. Shao^{60,48}, C. P. Shen⁹, P. X. Shen³⁷, X. Y. Shen^{1,52}, H. C. Shi^{60,48}, R. S. Shi^{1,52}, X. Shi^{1,48}, X. D. Shi^{60,48}, J. J. Song⁴¹, Q. Q. Song^{60,48}, W. M. Song²⁷, Y. X. Song^{38,k}, S. Sosio^{63A,63C}, S. Spataro^{63A,63C}, F. F. Sui⁴¹, G. X. Sun¹, J. F. Sun¹⁶, L. Sun⁶⁵, S. S. Sun^{1,52}, T. Sun^{1,52}, W. Y. Sun³⁵, Y. J. Sun^{60,48}, Y. K. Sun^{60,48}, Y. Z. Sun¹, Z. T. Sun¹, Y. H. Tan⁶⁵, Y. X. Tan^{60,48}, C. J. Tang⁴⁵, G. Y. Tang¹, J. Tang⁴⁹, V. Thoren⁶⁴, B. Tsednee²⁶, I. Uman^{51D}, B. Wang¹, B. L. Wang⁵², C. W. Wang³⁶, D. Y. Wang^{38,k}, H. P. Wang^{1,52}, K. Wang^{1,48}, L. L. Wang¹, M. Wang⁴¹, M. Z. Wang^{38,k}, Meng Wang^{1,52}, W. H. Wang⁶⁵, W. P. Wang^{60,48}, X. Wang^{38,k}, X. F. Wang³², X. L. Wang^{9,h}, Y. Wang⁴⁹, Y. Wang^{60,48}, Y. D. Wang¹⁵, Y. F. Wang^{1,48,52}, Y. Q. Wang¹, Z. Wang^{1,48}, Z. Y. Wang¹, Ziyi Wang⁵², Zongyuan Wang^{1,52}, D. H. Wei¹², P. Weidenkaff²⁸, F. Weidner⁵⁷, S. P. Wen¹, D. J. White⁵⁵, U. Wiedner⁴

G. Wilkinson⁵⁸, M. Wolke⁶⁴, L. Wollenberg⁴, J. F. Wu^{1,52}, L. H. Wu¹, L. J. Wu^{1,52}, X. Wu^{9,h}, Z. Wu^{1,48}, L. Xia^{60,48}, H. Xiao^{9,h}, S. Y. Xiao¹, Y. J. Xiao^{1,52}, Z. J. Xiao³⁵, X. H. Xie^{38,k}, Y. G. Xie^{1,48}, Y. H. Xie⁶, T. Y. Xing^{1,52}, X. A. Xiong^{1,52}, G. F. Xu¹, J. J. Xu³⁶, Q. J. Xu¹⁴, W. Xu^{1,52}, X. P. Xu⁴⁶, F. Yan^{9,h}, L. Yan^{9,h}, L. Yan^{63A,63C}, W. B. Yan^{60,48}, W. C. Yan⁶⁸, Xu Yan⁴⁶, H. J. Yang^{42,g}, H. X. Yang¹, L. Yang⁶⁵, R. X. Yang^{60,48}, S. L. Yang^{1,52}, Y. H. Yang³⁶, Y. X. Yang¹², Yifan Yang^{1,52}, Zhi Yang²⁵, M. Ye^{1,48}, M. H. Ye⁷, J. H. Yin¹, Z. Y. You⁴⁹, B. X. Yu^{1,48,52}, C. X. Yu³⁷, G. Yu^{1,52}, J. S. Yu^{20,l}, T. Yu⁶¹, C. Z. Yuan^{1,52}, W. Yuan^{63A,63C}, X. Q. Yuan^{38,k}, Y. Yuan¹, Z. Y. Yuan⁴⁹, C. X. Yue³³, A. Yuncu^{51B,a}, A. A. Zafar⁶², Y. Zeng^{20,l}, B. X. Zhang¹, Guangyi Zhang¹⁶, H. H. Zhang⁴⁹, H. Y. Zhang^{1,48}, J. L. Zhang⁶⁶, J. Q. Zhang⁴, J. W. Zhang^{1,48,52}, J. Y. Zhang¹, J. Z. Zhang^{1,52}, Jianyu Zhang^{1,52}, Jiawei Zhang^{1,52}, L. Zhang¹, Lei Zhang³⁶, S. Zhang⁴⁹, S. F. Zhang³⁶, T. J. Zhang^{42,g}, X. Y. Zhang⁴¹, Y. Zhang⁵⁸, Y. H. Zhang^{1,48}, Y. T. Zhang^{60,48}, Yan Zhang^{60,48}, Yao Zhang¹, Yi Zhang^{9,h}, Z. H. Zhang⁶, Z. Y. Zhang⁶⁵, G. Zhao¹, J. Zhao³³, J. Y. Zhao^{1,52}, J. Z. Zhao^{1,48}, Lei Zhao^{60,48}, Ling Zhao¹, M. G. Zhao³⁷, Q. Zhao¹, S. J. Zhao⁶⁸, Y. B. Zhao^{1,48}, Y. X. Zhao²⁵, Z. G. Zhao^{60,48}, A. Zhemchugov^{29,b}, B. Zheng⁶¹, J. P. Zheng^{1,48}, Y. Zheng^{38,k}, Y. H. Zheng⁵², B. Zhong³⁵, C. Zhong⁶¹, L. P. Zhou^{1,52}, Q. Zhou^{1,52}, X. Zhou⁶⁵, X. K. Zhou⁵², X. R. Zhou^{60,48}, A. N. Zhu^{1,52}, J. Zhu³⁷, K. Zhu¹, K. J. Zhu^{1,48,52}, S. H. Zhu⁵⁹, W. J. Zhu³⁷, X. L. Zhu⁵⁰, Y. C. Zhu^{60,48}, Z. A. Zhu^{1,52}, B. S. Zou¹, J. H. Zou¹

(BESIII Collaboration)

¹ Institute of High Energy Physics, Beijing 100049, People's Republic of China

² Beihang University, Beijing 100191, People's Republic of China

³ Beijing Institute of Petrochemical Technology, Beijing 102617, People's Republic of China

⁴ Bochum Ruhr-University, D-44780 Bochum, Germany

⁵ Carnegie Mellon University, Pittsburgh, Pennsylvania 15213, USA

⁶ Central China Normal University, Wuhan 430079, People's Republic of China

⁷ China Center of Advanced Science and Technology, Beijing 100190, People's Republic of China

⁸ COMSATS University Islamabad, Lahore Campus, Defence Road, Off Raiwind Road, 54000 Lahore, Pakistan

⁹ Fudan University, Shanghai 200443, People's Republic of China

¹⁰ G.I. Budker Institute of Nuclear Physics SB RAS (BINP), Novosibirsk 630090, Russia

¹¹ GSI Helmholtzcentre for Heavy Ion Research GmbH, D-64291 Darmstadt, Germany

¹² Guangxi Normal University, Guilin 541004, People's Republic of China

¹³ Guangxi University, Nanning 530004, People's Republic of China

¹⁴ Hangzhou Normal University, Hangzhou 310036, People's Republic of China

¹⁵ Helmholtz Institute Mainz, Johann-Joachim-Becher-Weg 45, D-55099 Mainz, Germany

¹⁶ Henan Normal University, Xinxiang 453007, People's Republic of China

¹⁷ Henan University of Science and Technology, Luoyang 471003, People's Republic of China

¹⁸ Huangshan College, Huangshan 245000, People's Republic of China

¹⁹ Hunan Normal University, Changsha 410081, People's Republic of China

²⁰ Hunan University, Changsha 410082, People's Republic of China

²¹ Indian Institute of Technology Madras, Chennai 600036, India

²² Indiana University, Bloomington, Indiana 47405, USA

²³ (A)INFN Laboratori Nazionali di Frascati, I-00044, Frascati, Italy; (B)INFN Sezione

di Perugia, I-06100, Perugia, Italy; (C)University of Perugia, I-06100, Perugia, Italy

²⁴ (A)INFN Sezione di Ferrara, I-44122, Ferrara, Italy; (B)University of Ferrara, I-44122, Ferrara, Italy

²⁵ Institute of Modern Physics, Lanzhou 730000, People's Republic of China

²⁶ Institute of Physics and Technology, Peace Ave. 54B, Ulaanbaatar 13330, Mongolia

²⁷ Jilin University, Changchun 130012, People's Republic of China

²⁸ Johannes Gutenberg University of Mainz, Johann-Joachim-Becher-Weg 45, D-55099 Mainz, Germany

²⁹ Joint Institute for Nuclear Research, 141980 Dubna, Moscow region, Russia

³⁰ Justus-Liebig-Universitaet Giessen, II. Physikalisches Institut, Heinrich-Buff-Ring 16, D-35392 Giessen, Germany

³¹ KVI-CART, University of Groningen, NL-9747 AA Groningen, The Netherlands

³² Lanzhou University, Lanzhou 730000, People's Republic of China

³³ Liaoning Normal University, Dalian 116029, People's Republic of China

³⁴ Liaoning University, Shenyang 110036, People's Republic of China

³⁵ Nanjing Normal University, Nanjing 210023, People's Republic of China
³⁶ Nanjing University, Nanjing 210093, People's Republic of China
³⁷ Nankai University, Tianjin 300071, People's Republic of China
³⁸ Peking University, Beijing 100871, People's Republic of China
³⁹ Qufu Normal University, Qufu 273165, People's Republic of China
⁴⁰ Shandong Normal University, Jinan 250014, People's Republic of China
⁴¹ Shandong University, Jinan 250100, People's Republic of China
⁴² Shanghai Jiao Tong University, Shanghai 200240, People's Republic of China
⁴³ Shanxi Normal University, Linfen 041004, People's Republic of China
⁴⁴ Shanxi University, Taiyuan 030006, People's Republic of China
⁴⁵ Sichuan University, Chengdu 610064, People's Republic of China
⁴⁶ Soochow University, Suzhou 215006, People's Republic of China
⁴⁷ Southeast University, Nanjing 211100, People's Republic of China
⁴⁸ State Key Laboratory of Particle Detection and Electronics,
 Beijing 100049, Hefei 230026, People's Republic of China
⁴⁹ Sun Yat-Sen University, Guangzhou 510275, People's Republic of China
⁵⁰ Tsinghua University, Beijing 100084, People's Republic of China
⁵¹ (A)Ankara University, 06100 Tandoğan, Ankara, Turkey; (B)Istanbul Bilgi
 University, 34060 Eyüp, İstanbul, Turkey; (C)Uludag University, 16059 Bursa,
 Turkey; (D)Near East University, Nicosia, North Cyprus, Mersin 10, Turkey
⁵² University of Chinese Academy of Sciences, Beijing 100049, People's Republic of China
⁵³ University of Hawaii, Honolulu, Hawaii 96822, USA
⁵⁴ University of Jinan, Jinan 250022, People's Republic of China
⁵⁵ University of Manchester, Oxford Road, Manchester, M13 9PL, United Kingdom
⁵⁶ University of Minnesota, Minneapolis, Minnesota 55455, USA
⁵⁷ University of Muenster, Wilhelm-Klemm-Str. 9, 48149 Muenster, Germany
⁵⁸ University of Oxford, Keble Rd, Oxford, UK OX13RH
⁵⁹ University of Science and Technology Liaoning, Anshan 114051, People's Republic of China
⁶⁰ University of Science and Technology of China, Hefei 230026, People's Republic of China
⁶¹ University of South China, Hengyang 421001, People's Republic of China
⁶² University of the Punjab, Lahore-54590, Pakistan
⁶³ (A)University of Turin, I-10125, Turin, Italy; (B)University of Eastern
 Piedmont, I-15121, Alessandria, Italy; (C)INFN, I-10125, Turin, Italy
⁶⁴ Uppsala University, Box 516, SE-75120 Uppsala, Sweden
⁶⁵ Wuhan University, Wuhan 430072, People's Republic of China
⁶⁶ Xinyang Normal University, Xinyang 464000, People's Republic of China
⁶⁷ Zhejiang University, Hangzhou 310027, People's Republic of China
⁶⁸ Zhengzhou University, Zhengzhou 450001, People's Republic of China
^a Also at Bogazici University, 34342 Istanbul, Turkey
^b Also at the Moscow Institute of Physics and Technology, Moscow 141700, Russia
^c Also at the Novosibirsk State University, Novosibirsk, 630090, Russia
^d Also at the NRC "Kurchatov Institute", PNPI, 188300, Gatchina, Russia
^e Also at Istanbul Arel University, 34295 Istanbul, Turkey
^f Also at Goethe University Frankfurt, 60323 Frankfurt am Main, Germany
^g Also at Key Laboratory for Particle Physics, Astrophysics and Cosmology, Ministry
 of Education; Shanghai Key Laboratory for Particle Physics and Cosmology; Institute
 of Nuclear and Particle Physics, Shanghai 200240, People's Republic of China
^h Also at Key Laboratory of Nuclear Physics and Ion-beam Application (MOE) and Institute
 of Modern Physics, Fudan University, Shanghai 200443, People's Republic of China
ⁱ Also at Harvard University, Department of Physics, Cambridge, MA, 02138, USA
^j Currently at: Institute of Physics and Technology, Peace Ave.54B, Ulaanbaatar 13330, Mongolia

^k Also at State Key Laboratory of Nuclear Physics and Technology,
Peking University, Beijing 100871, People's Republic of China

^l School of Physics and Electronics, Hunan University, Changsha 410082, China

Using 2.93 fb^{-1} of e^+e^- collision data taken at a center-of-mass energy of 3.773 GeV with the BESIII detector, we report the first measurements of the absolute branching fractions of fourteen hadronic $D^{0(+)}$ decays to exclusive final states with an η , e.g., $D^0 \rightarrow K^-\pi^+\eta$, $K_S^0\pi^0\eta$, $K^+K^-\eta$, $K_S^0K_S^0\eta$, $K^-\pi^+\pi^0\eta$, $K_S^0\pi^+\pi^-\eta$, $K_S^0\pi^0\pi^0\eta$, and $\pi^+\pi^-\pi^0\eta$; $D^+ \rightarrow K_S^0\pi^+\eta$, $K_S^0K^+\eta$, $K^-\pi^+\pi^+\eta$, $K_S^0\pi^+\pi^0\eta$, $\pi^+\pi^+\pi^-\eta$, and $\pi^+\pi^0\pi^0\eta$. Among these decays, the $D^0 \rightarrow K^-\pi^+\eta$ and $D^+ \rightarrow K_S^0\pi^+\eta$ decays have the largest branching fractions, which are $\mathcal{B}(D^0 \rightarrow K^-\pi^+\eta) = (1.853 \pm 0.025_{\text{stat}} \pm 0.031_{\text{syst}})\%$ and $\mathcal{B}(D^+ \rightarrow K_S^0\pi^+\eta) = (1.309 \pm 0.037_{\text{stat}} \pm 0.031_{\text{syst}})\%$, respectively. We also determine the CP asymmetries for the six decays with highest event yields. No evidence of CP violation is found.

PACS numbers: 13.20.Fc, 14.40.Lb

Hadronic D decays provide an ideal platform to explore strong and weak effects in decays of hadrons with charm or bottom quarks. Tests of lepton flavor universality (LFU) with semileptonic B decays are important to explore new physics beyond the SM. In recent years, the branching fraction (BF) ratios $\mathcal{R}_{\tau/\ell} = \mathcal{B}_{B \rightarrow \bar{D}^{(*)}\tau^+\bar{\nu}_\tau}/\mathcal{B}_{B \rightarrow \bar{D}^{(*)}\ell^+\bar{\nu}_\ell}$ ($\ell = \mu, e$) measured by BaBar, Belle, and LHCb [1–8] were found to deviate from the standard model (SM) prediction by 3.1σ [9]. It is argued in Ref. [10] that the exclusive hadronic $D^{0(+)}$ decays to η are key potential backgrounds in these tests. However, the known exclusive D^0 and D^+ decays to final states with an η meson only account for 44% and 16% of their corresponding inclusive rates [11], respectively. In particular, the BFs for the decays $D \rightarrow \bar{K}\pi\eta$, $K\bar{K}\eta$, $\bar{K}\pi\pi\eta$, and $\pi\pi\pi\eta$ (excluding narrow peaks K_S^0 , η , ω , η' , and ϕ in individual mass spectra) are poorly known, except for relative measurements of $D^0 \rightarrow K^-\pi^+\eta$ [12] and $D^0 \rightarrow K_S^0\pi^0\eta$ [13]. Measurements of the BFs of these decays are crucial to address the tensions found in LFU tests with semileptonic B decays. Furthermore, combining the measured BFs with the corresponding amplitude analysis results gives important information on two-body hadronic D decays. This is essential for improving the understanding of quark U-spin [14–16] and SU(3)-flavor symmetry breaking effects, thereby benefiting theoretical predictions of $D^0\bar{D}^0$ mixing and charge-parity (CP) violation in D decays [16–23].

Studies of CP violation in the weak decays of hadrons are powerful tools for understanding physics within the SM and searches for physics beyond it. The CP violation in D decays is predicted to be up to a few times 10^{-3} [23–29] and has been recently observed to be $(1.54 \pm 0.29) \times 10^{-3}$ in $D^0 \rightarrow K^+K^-$ and $\pi^+\pi^-$ decays by LHCb [30]. However, knowledge of CP violation in D decays is still very limited. Searching for CP asymmetries in hadronic D decays, which have been much less explored than (semi-)leptonic decays, allows for a more comprehensive understanding of CP violation in the D sector.

This Letter reports the first measurements of the absolute BFs for the decays $D^0 \rightarrow K^-\pi^+\eta$, $K_S^0\pi^0\eta$,

$K^+K^-\eta$, $K_S^0K_S^0\eta$, $K^-\pi^+\pi^0\eta$, $K_S^0\pi^+\pi^-\eta$, $K_S^0\pi^0\pi^0\eta$, $\pi^+\pi^-\pi^0\eta$, and $D^+ \rightarrow K_S^0\pi^+\eta$, $K_S^0K^+\eta$, $K^-\pi^+\pi^+\eta$, $K_S^0\pi^+\pi^0\eta$, $\pi^+\pi^+\pi^-\eta$, $\pi^+\pi^0\pi^0\eta$. Throughout this Letter, the charge conjugate processes are implied unless stated otherwise. In addition, the CP asymmetries are determined for the six decays with the highest yields. To avoid double-counting previously measured decays, the narrow peaks for the K_S^0 , η , ω , η' , and ϕ are removed from the mass spectra of the $\pi^{+(0)}\pi^{-(0)}$, $\pi^+\pi^-\pi^0$, $\pi^+\pi^-\pi^0$, $\pi^{+(0)}\pi^{-(0)}\eta$, and $K^+K^-(\pi^+\pi^-\pi^0)$ combinations, respectively.

The data sample was collected with the BESIII detector at a center-of-mass energy $\sqrt{s} = 3.773 \text{ GeV}$ and has an integrated luminosity of 2.93 fb^{-1} [31]. Details about the design and performance of the BESIII detector are given in Ref. [32]. The Monte Carlo (MC) simulated events are produced with a GEANT4-based [33] detector simulation software package. An inclusive MC sample, including $D^0\bar{D}^0$, D^+D^- , and non- $D\bar{D}$ decays of the $\psi(3770)$, initial state radiation (ISR) production of the $\psi(3686)$ and J/ψ , and the processes $e^+e^- \rightarrow q\bar{q}$ ($q = u, d, s$) and $e^+e^- \rightarrow (\gamma)\ell^+\ell^-$ ($\ell = e, \mu, \tau$), is produced to determine the detection efficiencies and to estimate any potential backgrounds. The production of the charmonium states is simulated by the MC generator KKMC [34]. The measured decay modes of the charmonium states are generated using EVTGEN [35] with BFs from the Particle Data Group [11], and the remaining unknown decay modes are generated by LUNDCHARM [36].

The BFs of the hadronic D (D^0 or D^+) decays are measured via the reaction chain $e^+e^- \rightarrow \psi(3770) \rightarrow D\bar{D}$. If a \bar{D} meson is fully reconstructed, it is called a single-tag (ST) \bar{D} meson. The ST D^- mesons are reconstructed via the decays $D^- \rightarrow K^+\pi^-\pi^-$, $K_S^0\pi^-$, $K^+\pi^-\pi^-\pi^0$, $K_S^0\pi^-\pi^0$, $K_S^0\pi^+\pi^-\pi^-$, and $K^+K^-\pi^-$, while the ST \bar{D}^0 mesons are reconstructed using the decays $\bar{D}^0 \rightarrow K^+\pi^-$, $K^+\pi^-\pi^0$, and $K^+\pi^-\pi^-\pi^+$. If a signal decay is fully reconstructed in the system recoiling against an ST \bar{D} meson, the candidate event is called a double-tag (DT)

event. The BF of the signal decay is given by

$$\mathcal{B}_{\text{sig}} = N_{\text{DT}} / (N_{\text{ST}} \cdot \epsilon_{\text{sig}}), \quad (1)$$

where $N_{\text{ST}} = \sum_i N_{\text{ST}}^i$ and N_{DT} are the total ST and DT yields in data, respectively, and $\epsilon_{\text{sig}} = \sum_i (N_{\text{ST}}^i \cdot \epsilon_{\text{DT}}^i / \epsilon_{\text{ST}}^i) / N_{\text{ST}}$ is the effective efficiency for detecting the signal decay, averaged over tag mode i , where ϵ_{ST} and ϵ_{DT} are the efficiencies for detecting ST and DT candidates, respectively.

We use the same selection criteria for K^\pm , π^\pm , K_S^0 , γ , and π^0 as were used in Refs. [37–43]. Candidates for η are reconstructed from $\gamma\gamma$ pairs with invariant mass within $(0.515, 0.570) \text{ GeV}/c^2$. To improve resolution, a one-constraint kinematic fit is imposed on each $\gamma\gamma$ pair to constrain their invariant mass at η nominal mass [11]. For $\bar{D}^0 \rightarrow K^+ \pi^- \pi^- \pi^+$ tags, the $\bar{D}^0 \rightarrow K_S^0 K^\pm \pi^\mp$ decays are rejected if the mass of any $\pi^+ \pi^-$ pair falls in the range $(0.478, 0.518) \text{ GeV}/c^2$.

Tagged \bar{D} (signal D) mesons are identified by two variables, the energy difference $\Delta E_{\text{tag(sig)}} \equiv E_{\text{tag(sig)}} - E_b$ and the beam-constrained mass $M_{\text{BC}}^{\text{tag(sig)}} \equiv \sqrt{E_b^2 - |\vec{p}_{\text{tag(sig)}}|^2}$, where tag (sig) represents the tagged \bar{D} (signal D), E_b the beam energy, and $\vec{p}_{\text{tag(sig)}}$ and $E_{\text{tag(sig)}}$ the momentum and energy of the \bar{D} (D) candidate in the e^+e^- rest frame. For each tag (signal) mode, if there are multiple combinations, only the one with the minimum $|\Delta E_{\text{tag(sig)}}|$ is kept for further analysis. The \bar{D} tags are required to satisfy $\Delta E_{\text{tag}} \in (-55, 40) \text{ MeV}$ for the modes containing π^0 in the final states and $\Delta E_{\text{tag}} \in (-25, 25) \text{ MeV}$ for the other modes. The yields of ST \bar{D} mesons are obtained from maximum binned likelihood fits to the $M_{\text{BC}}^{\text{tag}}$ distributions of the accepted ST candidates following Refs. [37–41]. The total ST D^- yield is $N_{\text{ST}D^-} = 1558159 \pm 2113_{\text{stat}}$. The total ST \bar{D}^0 yield is $N_{\text{ST}\bar{D}^0} = 2327839 \pm 1860_{\text{stat}}$ for self-conjugate signal D^0 decays. For the flavor specific signal decays $D^0 \rightarrow K^- \pi^+ \eta$ and $K^- \pi^+ \pi^0 \eta$, we remove doubly Cabibbo suppressed decays from the ST selection, giving $N_{\text{ST}\bar{D}^0} = 2321430 \pm 1860_{\text{stat}}$ for these decays.

For the signal D decays recoiling against the \bar{D} tags, tracks are selected from the residual tracks that have not been used for the tag reconstruction. The signal D decays are selected by using the ΔE_{sig} requirements as listed in Table 1. For the $\pi^+ \pi^- [\pi^0 \pi^0]$, $\pi^+ \pi^- \pi^0$, $\pi^+ \pi^- \pi^0$, $\pi^{+(0)} \pi^{-(0)} \eta$, and $K^+ K^-$ combinations, the K_S^0 , η , ω , η' , and ϕ contributions are rejected by requiring their invariant masses to be outside $(0.468, 0.528) \text{ GeV}/c^2$ $[(0.438, 0.538) \text{ GeV}/c^2]$, $(0.498, 0.578) \text{ GeV}/c^2$, $(0.732, 0.832) \text{ GeV}/c^2$, $(0.908, 1.008) \text{ GeV}/c^2$, and $(0.990, 1.390) \text{ GeV}/c^2$, respectively. These correspond to at least five times the fitted mass resolution away from individual nominal mass. For $D^0 \rightarrow K_S^0 \pi^{+(0)} \pi^{-(0)} \eta$ [$\pi^+ \pi^- \pi^0 \eta$] decays, no aforementioned mass requirements of the $K_S^0 [\phi]$ are imposed on the $\pi^{+(0)} \pi^{-(0)} [\pi^+ \pi^- \pi^0]$

combinations, due to the small BFs and the limited phase space (PHSP) of the background channels $D^0 \rightarrow K_S^0 K_S^0 \eta$ [$\phi \eta$]. The opening angle between signal D and tagged \bar{D} is required to be greater than 160° , with a loss of (2-6)% of the signal, to suppress mis-formed $D\bar{D}$ candidates. For $D \rightarrow \bar{K} \pi \pi^0 \eta$, the backgrounds of $D \rightarrow \bar{K} \pi \pi^0 \pi^0$ are rejected if any $\bar{K} \pi \pi^0 \pi^0$ combinations satisfying $\Delta E_{\bar{K} \pi \pi^0 \pi^0} \in (-0.05, 0.05) \text{ GeV}$ and $M_{\text{BC}}^{\bar{K} \pi \pi^0 \pi^0} \in (1.83, 1.89) \text{ GeV}/c^2$ can be found in the same candidate events. The combination of these requirements rejects more than 75% of the background and keeps (93-97)% of the signal.

To determine the DT yields in the data ($N_{\text{DT}}^{\text{fit}}$), a two-dimensional (2D) unbinned maximum likelihood fit is performed on the $M_{\text{BC}}^{\text{tag}}$ vs. $M_{\text{BC}}^{\text{sig}}$ distribution of the accepted DT candidates (See Fig. 1 of the supplemental material [44] for an example). Signal events concentrate around $M_{\text{BC}}^{\text{tag}} = M_{\text{BC}}^{\text{sig}} = M_D$, where M_D is the nominal D mass [11]. Background events are divided into three categories. The first one (named BKG I) is from events with correctly reconstructed D (\bar{D}) and incorrectly reconstructed \bar{D} (D). They are spread along the lines around $M_{\text{BC}}^{\text{tag}}$ or $M_{\text{BC}}^{\text{sig}} = M_D$. The second one (named BKG II) is from events smeared along the diagonal, which are mainly from the $e^+e^- \rightarrow q\bar{q}$ processes. The third one (named BKG III) comes from events with uncorrelated and incorrectly reconstructed D and \bar{D} .

In the 2D fit, the probability density functions (PDFs) of the backgrounds are constructed as

- BKG I: $b(x) \cdot c_y(y; E_b, \xi_y, \frac{1}{2}) + b(y) \cdot c_x(x; E_b, \xi_x, \frac{1}{2})$,
- BKG II: $c_z(z; \sqrt{2}E_b, \xi_z, \frac{1}{2}) \cdot g(k; 0, \sigma_k)$, and
- BKG III: $c_x(x; E_b, \xi_x, \frac{1}{2}) \cdot c_y(y; E_b, \xi_y, \frac{1}{2})$.

Here, $x = M_{\text{BC}}^{\text{sig}}$, $y = M_{\text{BC}}^{\text{tag}}$, $z = (x+y)/\sqrt{2}$, and $k = (x-y)/\sqrt{2}$. The PDFs for signal, $a(x, y)$, $b(x)$, and $b(y)$, are described by the corresponding MC-simulated shapes. $c_f(f; E_b, \xi_f, \frac{1}{2})$ is an ARGUS function [45] defined as $A_f \cdot f \cdot (1 - \frac{f^2}{E_b^2})^{\frac{1}{2}} \cdot e^{\xi_f(1 - \frac{f^2}{E_b^2})}$, where f denotes x , y , or z ; E_b is fixed at $1.8865 \text{ GeV}/c^2$; A_f is a normalization factor; and ξ_f is a fit parameter. $g(k; 0, \sigma_k)$ is a Gaussian function with mean of zero and standard deviation $\sigma_k = \sigma_0 \cdot (\sqrt{2}E_b - z)^p$, where σ_0 and p are two free parameters. For the decays $D^0 \rightarrow K_S^0 \pi^{+(0)} \pi^{-(0)} \eta$, $\pi^+ \pi^- \pi^0 \eta$, $K^- \pi^+ \pi^0 \eta$, $K_S^0 \pi^0 \eta$, and $D^+ \rightarrow K_S^0 \pi^+ \pi^0 \eta$, the yields and shapes of the peaking backgrounds mentioned above are fixed based on MC simulations. All other parameters are left free.

Combinatorial $\pi^+ \pi^-$ pairs can also satisfy the K_S^0 selection criteria and form peaking backgrounds around the D mass in the $M_{\text{BC}}^{\text{sig}}$ distribution. This kind of peaking background is estimated by the data events in the K_S^0 sideband region. For $D^0 \rightarrow K_S^0 \pi^0 \eta$, $K_S^0 \pi^+ \pi^- \eta$, $K_S^0 \pi^0 \eta$, and $D^+ \rightarrow K_S^0 \pi^+ \eta$, $K_S^0 K^+ \eta$, $K_S^0 \pi^+ \pi^0 \eta$,

one-dimensional (1D) signal and sideband regions are defined as $M_{\pi^+\pi^-} \in (0.486, 0.510) \text{ GeV}/c^2$ and $M_{\pi^+\pi^-} \in (0.454, 0.478) \cup (0.518, 0.542) \text{ GeV}/c^2$, respectively. For $D^0 \rightarrow K_S^0 K_S^0 \eta$, 2D signal and sideband regions are defined. The 2D sideband 1 (2) regions are defined as the boxes in which one (two) of the two $\pi^+\pi^-$ combinations lie in the K_S^0 sideband regions and the rest are located in the K_S^0 signal regions. See Fig. 2 of the supplemental material [44] as an example.

For the decays involving K_S^0 , the net DT yields are obtained by $N_{\text{DT}} = N_{\text{DT}}^{\text{fit}} - \frac{1}{2}N_{\text{sid-1}}^{\text{fit}} + \frac{1}{4}N_{\text{sid-2}}^{\text{fit}}$, where $N_{\text{DT}}^{\text{fit}}$ and $N_{\text{sid-}i}^{\text{fit}}$ are the fitted DT yields in the K_S^0 signal region and sideband i region, respectively. For the other decays, the net DT yields are $N_{\text{DT}}^{\text{fit}}$.

For each signal decay mode, the statistical significance is calculated by $\sqrt{-2\ln(\mathcal{L}_0/\mathcal{L}_{\text{max}})}$, where \mathcal{L}_{max} and \mathcal{L}_0 are the maximum likelihoods with and without the signal component in the fits, respectively. The effect of combinatorial $\pi^+\pi^-$ backgrounds in the K_S^0 signal regions has been considered for the decays involving K_S^0 . The statistical significances of the four decays with lowest yields, $D^0 \rightarrow K^+ K^- \eta$, $K_S^0 K_S^0 \eta$, $D^+ \rightarrow K_S^0 K^+ \eta$, and $K_S^0 \pi^+ \pi^0 \eta$, are 5.5σ , 2.8σ , 5.7σ , and 8.4σ , respectively; while those for the other decays are all greater than 10σ .

To determine the signal efficiencies (ϵ_{sig}), the $D \rightarrow \bar{K}\pi\eta$ decays are simulated with a modified data-driven generator BODY3 [35], which was developed to simulate different intermediate states in data for a given three-body final state. The Dalitz plot of $M_{K\pi}^2$ vs. $M_{\pi\eta}^2$ found in data, corrected for backgrounds and efficiencies, is taken as input for the BODY3 generator. The efficiencies across the kinematic space are obtained with MC samples generated with the PHSP generator. Intermediate states in the $D^0 \rightarrow K^+ K^- \eta$, $K_S^0 K_S^0 \eta$, $K_S^0 \pi^0 \pi^0 \eta$, and $D^+ \rightarrow K_S^0 K^+ \eta$, $K_S^0 \pi^+ \pi^0 \eta$ decays cannot be determined due to limited statistics; these decays are therefore simulated with the PHSP generator. Each of the other decays is simulated with a mixed signal MC sample. Here, the decays generated with PHSP generator and the decays containing $K^*(892)$, $\rho(770)$, and $a_0(980)$ intermediate states are mixed with fractions obtained by examining the corresponding invariant mass spectra. The data distributions for momenta and $\cos\theta$ (where θ is the polar angle in the e^+e^- rest frame) of the daughter particles, and the invariant masses of each of the two- and three-body particle combinations, agree with the MC simulations.

The values for N_{DT} , ϵ_{sig} , and the BFs of the signal decays are summarized in Table 1. The BF upper limit for $D^0 \rightarrow K_S^0 K_S^0 \eta$ at 90% confidence level is determined to be $< 2.4 \times 10^{-4}$, using the Bayesian approach after incorporating the systematic uncertainty [46].

The systematic uncertainties arise from the sources discussed below and are estimated relative to the measured BFs. The uncertainties in the total ST yields come from the $M_{\text{BC}}^{\text{tag}}$ fits to the ST \bar{D} candidates, which

Table 1. Requirements on ΔE_{sig} , net DT yields in data (N_{DT}), detection efficiencies (ϵ_{sig} , including the BFs of K_S^0 , η , and π^0 as well as correction factors described later), and the obtained BFs (\mathcal{B}_{sig}). Numbers in the first and second brackets are last two effective digits of statistical and systematic uncertainties, respectively, for \mathcal{B}_{sig} . The uncertainty is statistical only for N_{DT} .

Decay	ΔE_{sig} (MeV)	N_{DT}	ϵ_{sig} (%)	\mathcal{B}_{sig} ($\times 10^{-4}$)
$D^0 \rightarrow K^-\pi^+\eta$	(-37, 36)	6116.2 ± 81.8	14.22	$185.3(25)(31)$
$D^0 \rightarrow K_S^0 \pi^0 \eta$	(-57, 45)	1092.7 ± 35.2	4.66	$100.6(34)(30)$
$D^0 \rightarrow K^+ K^- \eta$	(-27, 27)	13.1 ± 4.0	9.53	$0.59(18)(05)$
$D^0 \rightarrow K_S^0 K_S^0 \eta$	(-29, 28)	7.3 ± 3.2	2.36	$1.33(59)(18)$
$D^0 \rightarrow K^-\pi^+\pi^0\eta$	(-44, 36)	576.5 ± 28.8	5.53	$44.9(22)(15)$
$D^0 \rightarrow K_S^0 \pi^+\pi^-\eta$	(-33, 32)	248.2 ± 18.0	3.80	$28.0(19)(10)$
$D^0 \rightarrow K_S^0 \pi^0 \pi^0 \eta$	(-56, 41)	64.7 ± 9.2	1.58	$17.6(23)(13)$
$D^0 \rightarrow \pi^+\pi^-\pi^0\eta$	(-57, 45)	508.6 ± 26.0	6.76	$32.3(17)(14)$
$D^+ \rightarrow K_S^0 \pi^+\eta$	(-36, 36)	1328.2 ± 37.8	6.51	$130.9(37)(31)$
$D^+ \rightarrow K_S^0 K^+\eta$	(-27, 27)	13.6 ± 3.9	4.72	$1.85(52)(08)$
$D^+ \rightarrow K^-\pi^+\pi^+\eta$	(-33, 33)	188.0 ± 15.3	8.94	$13.5(11)(04)$
$D^+ \rightarrow K_S^0 \pi^+\pi^0\eta$	(-49, 41)	48.7 ± 9.7	2.57	$12.2(24)(06)$
$D^+ \rightarrow \pi^+\pi^+\pi^-\eta$	(-40, 38)	514.6 ± 25.7	9.67	$34.1(17)(10)$
$D^+ \rightarrow \pi^+\pi^0\pi^0\eta$	(-70, 49)	192.5 ± 17.1	3.86	$32.0(28)(17)$

were determined as 0.5% for both neutral and charged \bar{D} [37–39]. The systematic uncertainties of the tracking efficiencies are found to be (0.2-0.5)% per K^\pm or π^\pm , while those for PID efficiencies are taken as (0.2-0.3)% per K^\pm or π^\pm , by using DT $D\bar{D}$ hadronic events. The systematic uncertainty in K_S^0 reconstruction is estimated to be 1.6% per K_S^0 by using the $J/\psi \rightarrow K^*(892)^\mp K^\pm$ and $J/\psi \rightarrow \phi K_S^0 K^\pm \pi^\mp$ candidates [47]. The systematic uncertainty of the π^0 reconstruction is assigned as (0.7-0.8)% per π^0 from studies of DT $D\bar{D}$ hadronic decay samples of $D^0 \rightarrow K^-\pi^+$, $K^-\pi^+\pi^+\pi^-$ vs. $\bar{D}^0 \rightarrow K^+\pi^-\pi^0$, $K_S^0 \pi^0$ [37, 38]. The systematic uncertainty for η reconstruction is taken to be the same as that for π^0 . The uncertainties of the quoted BFs of $K_S^0 \rightarrow \pi^+\pi^-$, $\eta \rightarrow \gamma\gamma$, and $\pi^0 \rightarrow \gamma\gamma$ decays are 0.07%, 0.5%, and 0.03% [11], respectively.

To estimate the systematic uncertainty in 2D fit, we repeat the fits by varying the signal shape and the endpoint of the ARGUS function. The systematic uncertainty of the $D\bar{D}$ opening angle requirement is assigned as 0.4% by using the DT events of $D^0 \rightarrow K^-\pi^+\pi^0$. The systematic uncertainty due to the ΔE_{sig} requirement is assigned to be 0.3%, which is the largest efficiency difference with and without smearing the data-MC Gaussian resolution of ΔE_{sig} for signal MC events. Here, the parameters of the Gaussian are obtained by using the DT samples of $D^0 \rightarrow K_S^0 \pi^0$, $K^-\pi^+\pi^0$, $K^-\pi^+\pi^0\pi^0$, and $D^+ \rightarrow K^-\pi^+\pi^+\pi^0$. The systematic uncertainties due to the choice of the K_S^0 sideband and the $K_S^0/\omega/\eta^{(\prime)}/\phi$ rejection windows are assigned

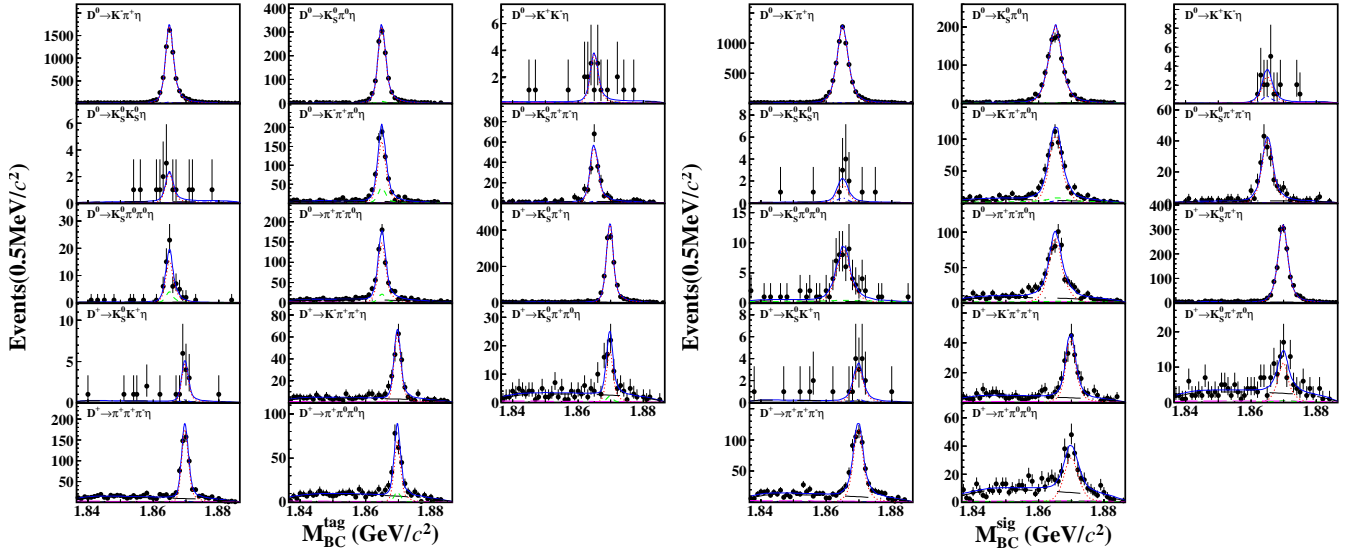


Fig. 1. Projections on M_{BC}^{tag} and M_{BC}^{sig} of the 2D fits to the DT candidate events. Data are shown as dots with error bars. Blue solid, red-dotted, blue dot-dashed, black dot-long-dashed, green long-dashed, and pink dashed curves denote the overall fit results, signal, BKG1, BKG2, BKG3, and peaking background components (see text), respectively.

by examining the changes of the BFs when varying the nominal K_S^0 sideband and rejection windows by ± 5 MeV/ c^2 . The uncertainties due to limited MC statistics (0.3-1.1)% are considered as a source of systematic uncertainty.

The systematic uncertainties in MC modeling are categorized into three cases. For the $D \rightarrow \bar{K}\pi\eta$ decays, the differences between the DT efficiencies obtained with the BODY3 and PHSP generators are assigned as the uncertainties. For the decays whose efficiencies are estimated with PHSP generator, the uncertainties are assigned by referring to the largest change of the efficiencies among $D^0 \rightarrow K^-\pi^+\eta$, $K_S^0\pi^0\eta$, and $D^+ \rightarrow K_S^0\pi^+\eta$. For the decays whose efficiencies are estimated with the mixed signal MC events, the systematic uncertainties are assigned as the change of the DT efficiency after removing the smallest component.

The $D^0\bar{D}^0$ pairs are produced coherently at the $\psi(3770)$. For the decays $D^0 \rightarrow K_S^0\pi^0\eta$, $K^+K^-\eta$, $K_S^0K^0\eta$, $K_S^0\pi^+\pi^-\eta$, $K_S^0\pi^0\pi^0\eta$, and $\pi^+\pi^-\pi^0\eta$, the measured BFs are affected by various CP components due to quantum-correlation (QC) effects. The fractions of $CP+$ components in these decays are examined by the $CP+$ tag of $D^0 \rightarrow K^+K^-$ and $CP-$ tag of $D^0 \rightarrow K_S^0\pi^0$, with the same method described in Ref. [48], and the necessary parameters are taken from Refs. [49-51]. The obtained impact of QC effects on the BFs (f_{QC}) is shown in Table 1 of the supplemental material [44]. The signal efficiencies are corrected by the corresponding f_{QC} factors, the residual statistical errors of f_{QC} are assigned as the systematic uncertainties.

For each signal decay, the total systematic uncertainty is obtained by adding the above effects in quadrature.

The systematic uncertainties for the various signal decays are given in Table 2 of the supplemental material [44].

For the six decay modes with the highest yields, the BFs of D and \bar{D} decays, $\mathcal{B}_{\text{sig}}^+$ and $\mathcal{B}_{\text{sig}}^-$, are measured separately. Their asymmetry is determined by $\mathcal{A}_{CP}^{\text{sig}} = \frac{\mathcal{B}_{\text{sig}}^+ - \mathcal{B}_{\text{sig}}^-}{\mathcal{B}_{\text{sig}}^+ + \mathcal{B}_{\text{sig}}^-}$. The obtained BFs and asymmetries are summarized in Table 2. No CP violation is found within the current statistics. Several systematic uncertainties cancel in the asymmetry: the tracking and PID of $\pi^+\pi^-/K^+K^-$ pair, K_S^0 reconstruction, π^0/η reconstruction, quoted BFs, K_S^0 sideband choice, $K_S^0/\omega/\eta'/\phi$ rejection windows, MC modeling, and strong phase of D^0 decays. The other systematic uncertainties are estimated separately as above.

Table 2. Charge-conjugated BFs ($\mathcal{B}_{\text{sig}}^+$ and $\mathcal{B}_{\text{sig}}^-$), and their asymmetries ($\mathcal{A}_{CP}^{\text{sig}}$). The first and second uncertainties are statistical and systematic, respectively, for $\mathcal{A}_{CP}^{\text{sig}}$; while uncertainties for $\mathcal{B}_{\text{sig}}^+$ and $\mathcal{B}_{\text{sig}}^-$ are only statistical.

Decay	$\mathcal{B}_{\text{sig}}^+ (\times 10^{-4})$	$\mathcal{B}_{\text{sig}}^- (\times 10^{-4})$	$\mathcal{A}_{CP}^{\text{sig}} (\%)$
$D^0 \rightarrow K^-\pi^+\eta$	182.1 ± 3.5	189.1 ± 3.6	$-1.9 \pm 1.3 \pm 1.0$
$D^0 \rightarrow K_S^0\pi^0\eta$	98.4 ± 4.8	106.3 ± 5.1	$-3.9 \pm 3.2 \pm 0.8$
$D^0 \rightarrow K^-\pi^+\pi^0\eta$	41.7 ± 2.7	48.8 ± 3.2	$-7.9 \pm 4.8 \pm 2.5$
$D^0 \rightarrow \pi^+\pi^-\pi^0\eta$	29.8 ± 2.2	33.3 ± 2.5	$-5.5 \pm 5.2 \pm 2.4$
$D^+ \rightarrow K_S^0\pi^+\eta$	129.9 ± 5.3	132.3 ± 5.4	$-0.9 \pm 2.9 \pm 1.0$
$D^+ \rightarrow \pi^+\pi^+\pi^-\eta$	35.4 ± 2.4	32.7 ± 2.4	$+2.5 \pm 5.0 \pm 1.6$

In summary, with 2.93 fb^{-1} of data taken at $\sqrt{s} = 3.773 \text{ GeV}$ with the BESIII detector, we report the first measurements of the absolute BFs of fourteen exclusive

$D^{0(+)}$ decays to η . Summing over the BFs measured in this work, and using the world averaged values of other known decays [11], the total BFs of all the exclusive D^0 and D^+ decays to η are determined to be $(8.62 \pm 0.35)\%$ and $(4.68 \pm 0.18)\%$, respectively. Here, the systematic uncertainties of N_{ST} , K^\pm/π^\pm tracking and PID, K_S^0 and η reconstruction, and the quoted BFs are correlated. They are consistent with the corresponding inclusive rates $(9.5 \pm 0.9)\%$ and $(6.5 \pm 0.7)\%$ within 0.9σ and 2.5σ , respectively, leaving little room for other exclusive decays involving η . The reported BFs provide key inputs for accurate background estimations in LFU tests with semileptonic B decays, which are crucial to explore possible new physics beyond the SM. The obtained $\mathcal{B}(D^0 \rightarrow K^-\pi^+\eta)$ agrees with the recent Belle result [11, 12] within 1.3σ , with precision improved twofold. Our $\mathcal{B}(D^0 \rightarrow K_S^0\pi^0\eta)$ is greater than CLEO's result [11, 13] by 3.7σ . Combining the measured $\mathcal{B}(D^0 \rightarrow K_S^0\pi^0\eta)$ with the fit fraction $\mathcal{B}(D^0 \rightarrow \bar{K}^*(892)^0\eta, \bar{K}^*(892)^0 \rightarrow K_S^0\pi^0)/\mathcal{B}(D^0 \rightarrow K_S^0\pi^0\eta)$ from CLEO [13], we find $\mathcal{B}(D^0 \rightarrow \bar{K}^*(892)^0\eta) = (1.77 \pm 0.44)\%$, where the uncertainty is dominated by the fit fraction. This deviates from various theoretical calculations [18, 19, 23] by $1.9\text{--}2.9\sigma$. Future amplitude analyses of these decays at BESIII [54] and Belle II [55] will open a window to extract more two-body hadronic D decays, which are important to understand quark U-spin and SU(3)-flavor symmetry breaking effects, and will be beneficial for the predictions of $D^0\bar{D}^0$ mixing and CP violation in D decays [18, 19, 23]. In addition, we determine the asymmetries of the charge-conjugated BFs for the six D decays with highest yields, and no CP violation is found with current statistics.

The BESIII collaboration thanks the staff of BEPCII and the IHEP computing center for their strong support. This work is supported in part by National Key Basic Research Program of China under Contract No. 2015CB856700; National Natural Science Foundation of China (NSFC) under Contracts Nos. 11775230, 11475123, 11625523, 11635010, 11735014, 11822506, 11835012, 11935015, 11935016, 11935018, 11961141012; the Chinese Academy of Sciences (CAS) Large-Scale Scientific Facility Program; Joint Large-Scale Scientific Facility Funds of the NSFC and CAS under Contracts Nos. U1532101, U1932102, U1732263, U1832207; CAS Key Research Program of Frontier Sciences under Contracts Nos. QYZDJ-SSW-SLH003, QYZDJ-SSW-SLH040; 100 Talents Program of CAS; INPAC and Shanghai Key Laboratory for Particle Physics and Cosmology; ERC under Contract No. 758462; German Research Foundation DFG under Contracts Nos. Collaborative Research Center CRC 1044, FOR 2359; Istituto Nazionale di Fisica Nucleare, Italy; Ministry of Development of Turkey under Contract No. DPT2006K-120470; National Science and Technology fund; STFC (United Kingdom); The Knut and Alice

Wallenberg Foundation (Sweden) under Contract No. 2016.0157; The Royal Society, UK under Contracts Nos. DH140054, DH160214; The Swedish Research Council; U. S. Department of Energy under Contracts Nos. DE-FG02-05ER41374, DE-SC-0012069.

- [1] J. P. Lees *et al.* (BaBar Collaboration), *Phys. Rev. Lett.* **109**, 101802 (2012).
- [2] J. P. Lees *et al.* (BaBar Collaboration), *Phys. Rev. D* **88**, 072012 (2013).
- [3] R. Aaij *et al.* (LHCb Collaboration), *Phys. Rev. Lett.* **115**, 111803 (2015).
- [4] M. Huschle *et al.* (Belle Collaboration), *Phys. Rev. D* **92**, 072014 (2015).
- [5] Y. Sato *et al.* (Belle Collaboration), *Phys. Rev. D* **94**, 072007 (2016).
- [6] R. Aaij *et al.* (LHCb Collaboration), *Phys. Rev. D* **97**, 072013 (2018).
- [7] A. Abdesselam *et al.* (Belle Collaboration), [arXiv:1904.08794](https://arxiv.org/abs/1904.08794).
- [8] G. Garia *et al.* (Belle collaboration), [arXiv:1910.05864](https://arxiv.org/abs/1910.05864).
- [9] Y. Amhis *et al.* (Heavy Flavor Averaging Group), [arXiv:1909.12524](https://arxiv.org/abs/1909.12524).
- [10] R. Aaij *et al.* (LHCb Collaboration), *Synergy of BESIII and LHCb physics programmes*, LHCb-PUB-2016-025.
- [11] M. Tanabashi *et al.* (Particle Data Group), *Phys. Rev. D* **98**, 030001 (2018) and 2019 update.
- [12] Y. Q. Chen *et al.* (Belle Collaboration), [arXiv:2003.07759](https://arxiv.org/abs/2003.07759).
- [13] P. Rubin *et al.* (CLEO Collaboration), *Phys. Rev. Lett.* **93**, 111801 (2004).
- [14] R. L. Kingsley, S. B. Treiman, F. Wilczek and A. Zee, *Phys. Rev. D* **11**, 1919 (1975).
- [15] M. Gronau, *Phys. Lett. B* **730**, 221 (2014); Erratum: *Phys. Lett. B* **735**, 282 (2014).
- [16] Z. Z. Xing, *Mod. Phys. Lett. A* **34**, 1950238 (2019).
- [17] H. J. Lipkin, *Phys. Rev. Lett.* **46**, 1307 (1981).
- [18] H. Y. Cheng and C. W. Chiang, *Phys. Rev. D* **81**, 074021 (2010).
- [19] Q. Qin, H. N. Li, C. D. Lü, and F. S. Yu, *Phys. Rev. D* **89**, 054006 (2014).
- [20] H. Y. Cheng, C. W. Chiang, and A. L. Kuo, *Phys. Rev. D* **93**, 114010 (2016).
- [21] W. Kwong and S. P. Rosen, *Phys. Lett. B* **298**, 413 (1993).
- [22] Y. Grossman and D. J. Robinson, *J. High Energy Phys.* **1304** (2013) 067.
- [23] H. N. Li, C. D. Lü, and F. S. Yu, *Phys. Rev. D* **86**, 036012 (2012).
- [24] I. I. Bigi, A. Paul, and S. Recksiegel, *J. High Energy Phys.* **1106** (2011) 089.
- [25] G. Isidori, J. F. Kamenik, Z. Ligeti, and G. Perez, *Phys. Lett. B* **711**, 46 (2011).
- [26] J. Brod, A. L. Kagan, and J. Zupan, *Phys. Rev. D* **86**, 014023 (2012).
- [27] H. Y. Cheng and C. W. Chiang, *Phys. Rev. D* **86**, 014014 (2012).
- [28] H. Y. Cheng and C. W. Chiang, *Phys. Rev. D* **100**, 093002 (2019).
- [29] H. N. Li, C. D. Lü, and F. S. Yu, [arXiv:1903.10638](https://arxiv.org/abs/1903.10638).

- [30] R. Aaij *et al.* (LHCb Collaboration), *Phys. Rev. Lett.* **122**, 211803 (2019).
- [31] M. Ablikim *et al.* (BESIII Collaboration), *Chin. Phys. C* **37**, 123001 (2013); *Phys. Lett. B* **753**, 629 (2016).
- [32] M. Ablikim *et al.* (BESIII Collaboration), *Nucl. Instrum. Meth. A* **614**, 345 (2010).
- [33] S. Agostinelli *et al.* (GEANT4 Collaboration), *Nucl. Instrum. Meth. A* **506**, 250 (2003).
- [34] S. Jadach, B. F. L. Ward, and Z. Was, *Phys. Rev. D* **63**, 113009 (2001); *Comput. Phys. Commun.* **130**, 260 (2000).
- [35] D. J. Lange, *Nucl. Instrum. Meth. A* **462**, 152 (2001); R. G. Ping, *Chin. Phys. C* **32**, 599 (2008).
- [36] J. C. Chen, G. S. Huang, X. R. Qi, D. H. Zhang, and Y. S. Zhu, *Phys. Rev. D* **62**, 034003 (2000).
- [37] M. Ablikim *et al.* (BESIII Collaboration), *Eur. Phys. J. C* **76**, 369 (2016).
- [38] M. Ablikim *et al.* (BESIII Collaboration), *Chin. Phys. C* **40**, 113001 (2016).
- [39] M. Ablikim *et al.* (BESIII Collaboration), *Phys. Rev. Lett.* **121**, 171803 (2018).
- [40] M. Ablikim *et al.* (BESIII Collaboration), *Phys. Rev. Lett.* **123**, 231801 (2019).
- [41] M. Ablikim *et al.* (BESIII Collaboration), *Phys. Rev. D* **101**, 052009 (2020).
- [42] M. Ablikim *et al.* (BESIII Collaboration), *Phys. Rev. D* **101**, 072005 (2020).
- [43] M. Ablikim *et al.* (BESIII Collaboration), *arXiv:2003.12220*.
- [44] See Supplemental Material at the link (to be added by editor) for an illustration of the M_{BC}^{tag} vs. M_{BC}^{sig} distribution, the definitions of 1D and 2D signal and sideband regions of K_S^0 , the correction factors due to QC effects, and the systematic uncertainties of various sources in the BF measurements.
- [45] H. Albrecht *et al.* (ARGUS Collaboration), *Phys. Lett. B* **241**, 278 (1990).
- [46] K. Stenson, *arXiv:physics/0605236*.
- [47] M. Ablikim *et al.* (BESIII Collaboration), *Phys. Rev. D* **92**, 112008 (2015).
- [48] M. Ablikim *et al.* (BESIII Collaboration), *Phys. Rev. D* **100**, 072006 (2019).
- [49] T. Gershon, J. Libby, and G. Wilkinson, *Phys. Lett. B* **750**, 338 (2015).
- [50] T. Evans *et al.*, *Phys. Lett. B* **757**, 520 (2016); Erratum: *Phys. Lett. B* **765**, 402 (2017).
- [51] Heavy Flavor Averaging Group (HFLAV), (<http://www.slac.stanford.edu/xorg/hflav/charm/>).
- [52] F. Buccella, M. Lusignoli, G. Miele, A. Pugliese, and P. Santorelli, *Phys. Rev. D* **51**, 3478 (1995); F. Buccella, M. Lusignoli, G. Mangano, G. Miele, A. Pugliese, and P. Santorelli, *Phys. Lett. B* **302**, 319 (1993).
- [53] F. S. Yu, X. X. Wang, and C. D. Lü, *Phys. Rev. D* **84**, 074019 (2011).
- [54] M. Ablikim *et al.* (BESIII Collaboration), *Chin. Phys. C* **40**, 040001 (2020).
- [55] E. Kou *et al.* (Belle II Collaboration), *PTEP* **2019**, 123C01 (2019).

SUPPLEMENTAL MATERIAL

Figure 1 shows the M_{BC}^{tag} vs. M_{BC}^{sig} distribution of the accepted DT candidate events.

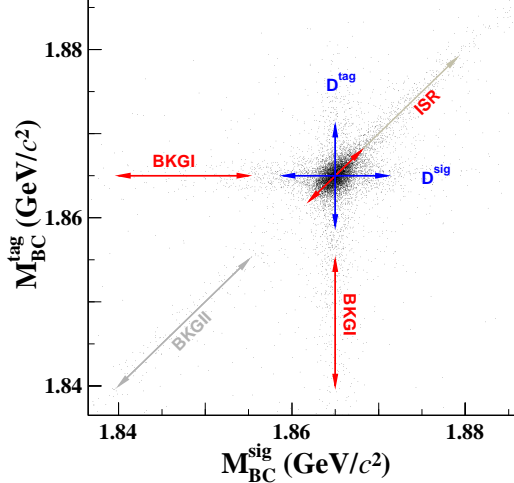


Fig. 1. The M_{BC}^{tag} vs. M_{BC}^{sig} distribution of the accepted DT candidate events.

Figure 2 shows the definitions of 1D and 2D K_S^0 signal and sideband regions.

Table 1 summarizes the ST yields of $CP\pm$ tags from the fits to the M_{BC}^{tag} distributions of the accepted ST candidates, the DT yields tagged by $CP\pm$ tags from the 2D fits to the M_{BC}^{tag} vs. M_{BC}^{sig} distributions of the accepted DT candidates, and the QC factors obtained with the same method as described in Ref. [48] and the necessary parameters quoted from Refs. [49–51]. No DT event are observed from the $D^0 \rightarrow K^+K^-\eta$ and $K_S^0K_S^0\eta$ decays. The systematic uncertainties arising from QC effects are directly assigned as the averaged strong-phase factor C_f by the flavor tag yields.

Table 2 summarizes the systematic uncertainties for various sources in the measurements of BFs, which are assigned relative to the measured BFs. For each signal decay, the total uncertainty is obtained by quadratically adding all errors.

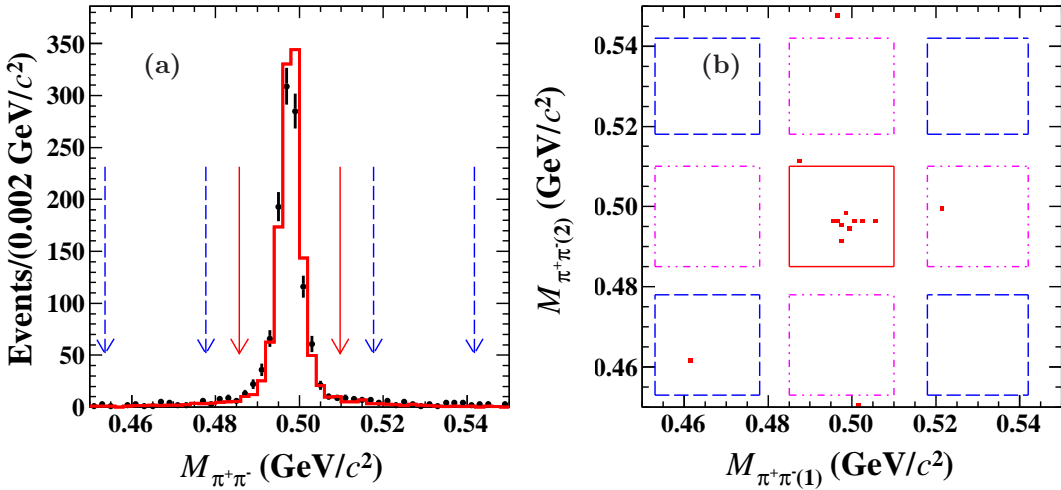


Fig. 2. (a) Comparison of the $M_{\pi^+\pi^-}$ distributions of the $D^0 \rightarrow K_S^0\pi^0\eta$ candidate events between data (dots with error bars) and the inclusive MC sample (histogram). Pairs of the solid (dashed) arrows denote the 1D K_S^0 signal (sideband) regions. (b) Distribution of $M_{\pi^+\pi^-_{(1)}}$ vs. $M_{\pi^+\pi^-_{(2)}}$ for the $D^0 \rightarrow K_S^0K_S^0\eta$ candidate events in data. Solid box denotes the 2D signal region. Dot-dashed (dashed) boxes indicate the 2D sideband 1 (2) regions.

Table 1. Summary of the ST yields of $CP\pm$ tags (S_{measured}^\pm), the DT yields tagged by $CP\pm$ tags (M_{measured}^\mp), and the QC factor (f_{QC}). The errors are statistical only.

CP tag	S_{measured}^+	S_{measured}^-	f_{QC}	Uncertainty (%)
	57779 ± 287	70512 ± 311		
Decay	M_{measured}^-	M_{measured}^+		
$D^0 \rightarrow K_S^0 \pi^0 \eta$	$2.4^{+1.6}_{-2.0}$	67.6 ± 8.3	$0.942^{+0.007}_{-0.008}$	0.8
$D^0 \rightarrow K^+ K^- \eta$	0	0	—	7.4
$D^0 \rightarrow K_S^0 K_S^0 \eta$	0	0	—	7.4
$D^0 \rightarrow K_S^0 \pi^+ \pi^- \eta$	19.8 ± 4.7	$2.0^{+0.9}_{-1.1}$	$1.057^{+0.013}_{-0.013}$	1.3
$D^0 \rightarrow K_S^0 \pi^0 \pi^0 \eta$	$5.4^{+2.8}_{-2.4}$	0	$1.073^{+0.065}_{-0.040}$	6.5
$D^0 \rightarrow \pi^+ \pi^- \pi^0 \eta$	13.6 ± 4.8	18.8 ± 4.4	$0.993^{+0.008}_{-0.008}$	0.8

Table 2. Systematic uncertainties (%) in the measurements of the BFs.

Sources	$D^0 \rightarrow$								$D^+ \rightarrow$							
	$K^- \pi^+ \eta$	$K_S^0 \pi^0 \eta$	$K^+ K^- \eta$	$K_S^0 K_S^0 \eta$	$K^- \pi^+ \pi^0 \eta$	$K_S^0 \pi^+ \pi^- \eta$	$K_S^0 \pi^0 \pi^0 \eta$	$\pi^+ \pi^- \pi^0 \eta$	$K_S^0 \pi^+ \eta$	$K_S^0 K^+ \eta$	$\pi^+ \pi^+ \pi^- \eta$	$\pi^+ \pi^0 \pi^0 \eta$	$K^- \pi^+ \pi^+ \eta$	$K_S^0 \pi^+ \pi^0 \eta$		
$N_{\text{ST}}^{\text{tot}}$	0.5	0.5	0.5	0.5	0.5	0.5	0.5	0.5	0.5	0.5	0.5	0.5	0.5	0.5	0.5	0.5
K^\pm/π^\pm tracking	0.7	—	1.0	—	0.9	0.7	—	0.6	0.2	0.5	1.2	0.4	0.9	0.3	—	—
K^\pm/π^\pm PID	0.4	—	0.5	—	0.4	0.4	—	0.4	0.2	0.3	0.7	0.2	0.6	0.2	—	—
π^0/η reconstruction	0.7	1.5	0.8	0.8	1.4	0.8	2.2	1.5	0.7	0.8	0.7	1.5	0.7	2.2	—	—
K_S^0 reconstruction	—	1.6	—	3.2	—	1.6	1.6	—	1.6	1.6	—	1.6	—	—	—	—
Quoted \mathcal{B}	0.5	0.5	0.5	0.5	0.5	0.5	0.5	0.5	0.5	0.5	0.5	0.5	0.5	0.5	0.5	0.5
2D fit	0.5	1.0	5.3	10.5	2.4	0.7	2.9	2.6	0.9	3.6	1.9	4.5	2.1	3.2	—	—
$D\bar{D}$ angle	0.4	0.4	0.4	0.4	0.4	0.4	0.4	0.4	0.4	0.4	0.4	0.4	0.4	0.4	0.4	0.4
ΔE^{sig} requirement	0.3	0.3	0.3	0.3	0.3	0.3	0.3	0.3	0.3	0.3	0.3	0.3	0.3	0.3	0.3	0.3
$K_S^0/\eta/\omega/\eta'$ rejection	—	—	—	—	—	3.7	5.9	2.3	—	—	—	—	1.9	2.9	—	—
K_S^0 sideband	—	0.5	—	—	—	0.6	—	—	0.2	—	—	—	—	—	—	—
MC statistics	0.3	0.5	0.4	0.6	0.5	0.6	1.1	0.5	0.4	0.5	0.4	0.7	0.4	0.7	0.4	0.7
MC generator	0.5	0.8	0.9	0.9	1.2	1.5	0.9	1.8	0.9	0.9	1.5	0.9	1.2	1.9	—	—
Strong phase of neutral D	—	0.8	7.4	7.4	—	1.3	6.5	0.8	—	—	—	—	—	—	—	—
Total	1.6	2.9	9.3	13.3	3.4	3.8	8.3	4.4	2.4	4.2	3.0	5.2	3.4	5.3		